ELSEVIER

Soil & Tillage Research 64 (2002) 41–59

Soil & Tillage Research

www.elsevier.com/locate/still

Review

Modeling post-tillage soil structural dynamics: a review

Dani Or*, Teamrat A. Ghezzehei[1]

Department of Plants, Soils and Biometeorology, Utah State University, Logan, UT 84322-4820, USA

Abstract

Tillage modifies the soil structure to create conditions favorable for plant growth. However, the resulting loose structure is susceptible to collapse by internal capillary forces and external compactive stresses with concurrent changes in soil hydraulic properties. Presently, limited understanding of these complex processes often leads to consideration of the soil plow-layer as a static porous medium. Our objective is to provide a review of recent progress in modeling soil structural dynamics at the pore-scale, based on soil mechanical and rheological properties. The basic geometrical framework of the models was a cubic arrangement of monosized spherical aggregates (other arrangements are discussed). The process of soil aggregate rejoining by capillary forces was modeled by considering the rate of energy dissipation due to viscous deformation of wet soil, and corresponding energy release due to reconfiguration of water capillary menisci. The model was complemented by independent rheological characterization of soil that provides control on the rate as well as the onset and termination of aggregate coalescence. The model was also adapted for consideration of steady stress (such as overburden) acting upon the unit cells. Unlike steady stress, transient stress (such as traffic) is applied for too short of a period to allow for total energy dissipation by viscous deformation. Hence, a portion of the deformation is elastic (with a recoverable portion of the applied energy). Rheological characterization under transient (oscillatory) stress provided coupled elastic and viscous properties under several loading frequencies. Effects of transient stresses on the geometrical model were modeled by considering a combination of (i) Hertzian-type elastic strain and (ii) viscous flow of soil at the contacts. Application of the models is demonstrated using illustrative examples and rheological measurements of Millville silt loam soil. Finally, we provide an outlook for upscaling the unit cell results to an aggregate bed scale.

Keywords: Rheology; Soil-structure; Compaction; Aggregate

1. Introduction

Tillage of agricultural soils creates favorable physical conditions for crop growth by modifying the soil structure in the plow layer. However, the desired loose soil tilth tends to be structurally unstable and is susceptible to collapse due to internal and external forces. The primary causes of structural deterioration in near-surface soils are: (i) mechanical compaction by agricultural implements; (ii) surface crusting due to raindrop impact and water ponding (Sumner and Stewart, 1992); (iii) subsurface rejoining of aggregates due to tensile forces of capillary water (Keller, 1970; Or, 1996; Silva, 1995). Soil structural dynamics considerably alter soil hydraulic and transport properties, as well as mechanical and thermal characteristics (Wiermann et al., 2000). The lack of adequate understanding of post-tillage soil structural dynamics leads to the erroneous assumption in most water and solute flow models of structurally stable porous media with

* Corresponding author. Tel.: +1-435-797-2637; fax: +1-435-797-2117.
E-mail addresses: dani@mendel.usu.edu (D. Or), teamrat@mendel.usu.edu (T.A. Ghezzehei).
[1] Tel.: +1-435-797-2175; fax: +1-435-797-2117.

0167-1987/02/$ – see front matter
PII: S0167-1987(01)00256-2

constant pore geometry throughout the flow process (Collis-George and Greene, 1979).

Traditionally, stress–strain relationships that rely on empirical geotechnical engineering practices have been used to study compaction of agricultural soils (Koolen, 1983). These approaches fail to address key features of soil structural dynamics required for modeling of subsequent evolution of hydraulic properties. Primarily, the empirical methods are not adequate for a priori prediction of soil structural changes (Hillel, 1998). Secondly, these approaches are based on equilibrium state stress–strain relations, while deformations in agricultural soils are often dynamic processes that rarely reach equilibrium (Or, 1996), especially when transient and rapid loading by agricultural machinery is considered. Finally, these methods are applicable for describing bulk volume changes only and not details of pore-scale processes crucial for flow and transport processes. Recently, we proposed an alternative approach that circumvents some of these limitations by considering pore-scale mechanistic models coupled with intrinsic soil rheological properties and stochastic upscaling (Ghezzehei and Or, 2000, 2001; Or, 1996; Or et al., 2000). These models address soil structural changes induced by internal capillary forces, and external steady and transient forces such as passage of a tractor. The objective of this paper is to provide a review of these developments with emphasis on their applications. Implementation of the models and acquisition of the required inputs are emphasized, while details of the underlying theories and mathematical derivations are omitted.

The paper is organized as follows: soil structural dynamics under steady and transient stresses are presented in Sections 2 and 3, respectively. Both sections consist of discussions on: (i) natural manifestation of the respective stresses; (ii) relevant soil rheological properties and applicable methods of determination; (iii) development of appropriate mechanistic models; (iv) illustrative examples. Finally, potentials for upscaling the models to aggregate beds and outlook for future research are presented in Section 4.

Distinction between steady and transient stresses was made based on the rate of change of stress relative to strain rate. Steady stress refers to slow change in inter-aggregate contact stress compared to the associated strain rate. In contrast, transient stress refers to comparable rate of change of inter-aggregate stress and strain rate.

2. Soil structural dynamics under steady stress

Steady stress in aggregated soils may arise from (i) capillary forces of water menisci between soil aggregates and/or (ii) external static loads (such as overburden). These stresses result in time-dependent soil structural evolution, dependent on the soil physical state and the magnitude and duration of the stress application. In this section, we will review applicable rheological principles and methods of soil rheological characterization followed by mechanistic modeling framework.

2.1. Rheological properties of wet soil under steady stress

2.1.1. Rheological principles

Viscosity is an intrinsic property of fluids to resist motion of elemental particles with respect to one another. In ideal Newtonian-fluids, viscous flow is induced by any shear stress greater than 0, and progresses at constant velocity $\dot{\gamma} = \mathrm{d}\gamma/\mathrm{d}t = \text{constant}$, where γ is shear strain and t the time. The shear velocity is directly proportional to the applied shear stress (τ):

$$\tau = \eta\dot{\gamma} \tag{1}$$

where η is the coefficient of viscosity. A perfectly plastic body, on the other hand, begins to change its shape when the maximum tangential stress ($\tau_{\max}$) attains ultimate stress value τ_s, termed the yield stress:

$$\tau_{\max} = \tau_s = \text{constant} \tag{2}$$

Microscopic study of aggregate welding processes indicates that flow of soil is initiated only when the stress acting upon the inter-aggregate contact exceeds a critical yielding point (Day and Holmgren, 1952; McMurdie and Day, 1958). Beyond the yield stress, soil aggregates flow in a manner similar to viscous material at a rate proportional to the stress in excess of the yield stress (Ghavami et al., 1974; Keller, 1970). This combination of plastic and viscous behaviors is commonly referred to as viscoplasticity.

Upon close examination of experimental stress–strain rate relationships of several soils, Vyalov (1986) has shown that wet soil begins to flow in a

manner similar to viscous fluids only when the applied stress exceeds a threshold stress value (τ_s). One of the simplest models that describes such mixed viscoplastic flow behavior is the Bingham rheological model, which states that plastic flow is possible only when the applied stress τ exceeds a critical (yield) stress τ_y, beyond which the flow obeys Newton's law (1). The equation of flow for a Bingham fluid is written as

$$\frac{\tau - \tau_y}{\eta_p} = \dot{\gamma} \tag{3}$$

provided that $\tau > \tau_y$. In terms of ''Newtonian'' viscosity, (3) may be written as

$$\eta = \eta_p + \frac{\tau_y}{\dot{\gamma}} \tag{4}$$

where η_p is the coefficient of plastic viscosity and η the instantaneous viscosity (that depends on the strain rate).

2.1.2. Experimental determination of soil viscoplasticity

Ghezzehei and Or (2001) used a rotational (torsional) rheometer, with a parallel-plate sensor system (RheoStress RS75, Gebrüder HAAKE GmbH, Germany) to determine soil rheological properties. The instrumental setup is shown in Fig. 1. The soil sample is placed between the rotary plate (top) and stationary plate (bottom) at a specified constant spacing (2 mm) between the plates. The shaft of the rotary plate is equipped with sensors that measure torque and angular velocity, and the computerized driver translates these measurements to average shear stress (τ) and shear strain (γ), respectively, using geometrical relations. During measurement, a controlled shear stress (τ) is applied to the sample, and the resulting shear strain (γ) and shear rate ($\dot{\gamma}$) are determined. The sample viscosity (η_p) and yield stress (τ_y) are derived from the flow curves according to (3). Measurements were conducted at several water content values.

The soil samples were sieved through 1.0 mm mesh size. Different water content levels were established for all samples by hand-mixing air-dried soil with an appropriate mass of water, and allowing the mixture to equilibrate for 48–72 h. For illustrative purposes, we report the rheological properties of Millville silt loam soil (sand, 29%; silt, 55%; clay, 16%) with kaolinitic and montmorillonitic clay mineralogy (73 $m^2\ g^{-1}$ area) (Or and Wraith, 1999). Measurements of more soils

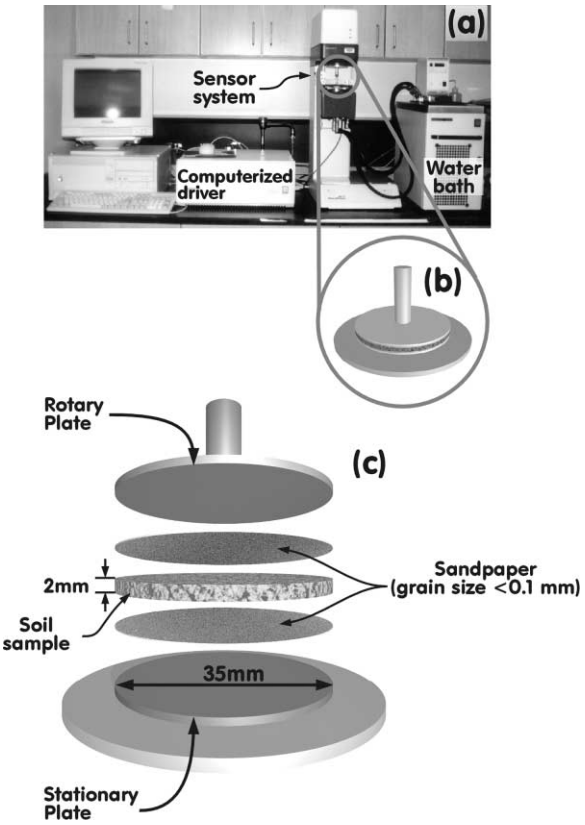

Fig. 1. Rotational rheometer: (a) complete setup; (b) sensor system during measurement; (c) arrangement of sandpaper and soil sample in sensor system.

and clays and detailed data analyses are given in (Ghezzehei and Or, 2001). Typical flow curves of Millville silt loam soil, determined at 0.28 and 0.34 kg/kg water content, and fitting of the Bingham rheological model are shown in Fig. 2.

These results show that yield stress (intercept) and viscosity (inverse slope of Bingham model) of Millville silt loam soil increase with decreasing water content. The models discussed in subsequent sections utilize these data for solving coalescence of soil aggregates under steady stress.

2.2. Capillary-induced aggregate coalescence

Tension wetting, in which the soil remains unsaturated, may develop under various conditions, such as low-intensity sprinkler irrigation (Keller, 1970) or even below the slaked surface layer under surface

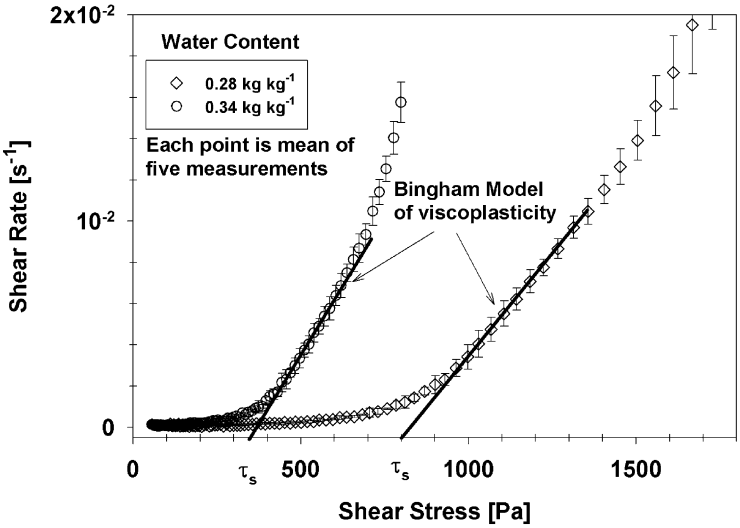

Fig. 2. Typical steady stress flow curves of Millville silt loam soil at 0.28 and 0.34 kg/kg water content.

irrigation. Unsaturated conditions result in enhanced aggregate cohesion by capillary forces (Kemper and Rosenau, 1984), whereas, the vented air pathways reduce destructive tensile forces exerted by entrapped air. Keller (1970) and coworkers have shown that under tension wetting, the wet soil losses it strength, and gradual structural changes take place through aggregate coalescence without the complete disintegration often observed in flooded surfaces (Mullins et al., 1990).

2.2.1. Welding of soil aggregates

Vomocil and Folker (1961) observed that reduction of inter-aggregate pores is the primary cause for the large volume changes (as much as 50%) observed following tillage. Unlike the rapid disintegration of aggregates on the soil *surface* during ponding and high intensity rainfall events, in partially saturated soils, *subsurface* reduction in porosity is carried out by welding of individual aggregates at their contact areas (Keller, 1970; Kwaad and Mücher, 1994). Microscopic studies of aggregated soil subjected to external stresses have indicated that reduction in pore space was largely attributed to plastic deformation of soil aggregates at their contact, and that soil aggregates behaved in a manner similar to *perfectly plastic grains* (Day and Holmgren, 1952; McMurdie and Day, 1958).

Plastic deformation at inter-aggregate contacts under cyclic wetting and drying is illustrated in Fig. 3. The dry aggregates in Fig. 3a were separated by mechanical sieving without crushing (2–4 mm in diameter). When subjected to successive wetting and drying cycles, the aggregates formed clusters of several aggregates due to welding at their contacts (Fig. 3b). Part of the inter-aggregate porosity was retained, but reduced in size. Further crushing of the dried clusters of aggregates (Fig. 3c) shows that the welded necks were as strong as the aggregates themselves and much of the original structure of individual aggregates remained clearly visible.

2.2.2. Geometrical model: spherical aggregates in cubic packing

In order to simplify the mathematical representation of the geometries and processes of aggregate coalescence, spherical aggregates of radius a are used as ideal depiction of soil aggregates as illustrated in Fig. 4. The stresses and strains are analyzed on an aggregate pair model (Fig. 4a and b). The center of each sphere has moved to the contact plane by a distance of h. Analyses of evolution of soil density and pore size require a spatial coordination of aggregates. In this study, simple cubic packing of equal-sized aggregates is used. Fig. 4c depicts a unit element before coalescence ($h = 0$). As coalescence proceeds, soil material flows radially outward from the contact points, forming smoothed solid-necks (i.e., minimum

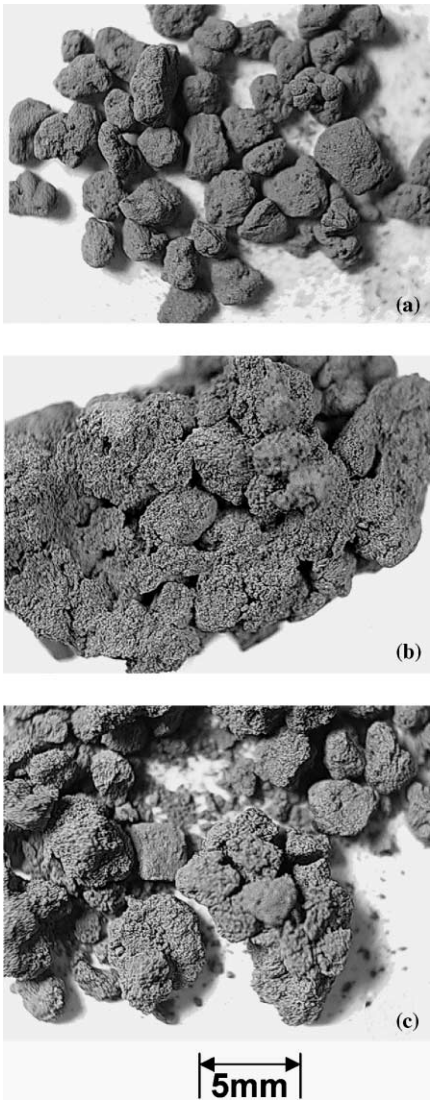

Fig. 3. Coalescence of Millville silt loam soil aggregates (2–4 mm) under wetting–drying cycles: (a) dry soil aggregates separated by mechanical sieving; (b) cluster of aggregates formed by coalescence due to wetting–drying cycles; (c) partly crushed cluster of aggregates. Note that coalescence took place mainly at the contact points, and most of the aggregates maintained part of their original boundaries.

energy configuration). Fig. 4d depicts a unit element after coalescence to 5% strain $(h/a = 0.05)$.

The caps of the spherical soil aggregates at the contacts are displaced from their original location to the periphery of the solid-neck by viscous flow. The cross-sectional contact area between the pair of aggregates evolves from a point into a circular plane of radius (x) as observed by Day and Holmgren (1952). The liquid–vapor menisci of isolated liquid elements in the neck area maintain minimum energy configuration and are described by the radii of curvature r and ρ. The pressure differential across the liquid–vapor interface (equivalent to matric potential) is given by the Laplace–Young equation

$$\psi = \sigma_{LV}\left(\frac{1}{r} - \frac{1}{\rho}\right) \tag{5}$$

where ψ is the matric potential in Pa and σ_{LV} the surface tension of the liquid–vapor interface. In order to keep r and ρ as positive geometrical quantities, the sign of the curvature is included in (5). For all further analyses, we assume that (i) the aggregates (spheres) are isotropic with respect to their physical properties, density, water content and internal matric potential, (ii) soil does not have a significant shrink–swell property and (iii) the change in density of individual aggregates during coalescence is negligible.

2.2.3. Energy relationships of capillary water

In partially saturated aggregated soils, individual soil aggregates experience cohesion due to the presence of liquid menisci at their contact points. For a pair of spherical aggregates, the cohesive force (F) is given by (Gessinger and Fischmeister, 1972; Heady and Cahn, 1970; Kemper and Rosenau, 1984)

$$F = 2\pi r\sigma_{LV} + \pi(r^2 - p^2)\psi \tag{6}$$

The first term on the right-hand side is due to the surface tension of the liquid (σ_{LV}) acting across the periphery of the liquid neck (denoted by F_σ in Fig. 4a). The second term is due to hydrostatic pressure difference across the liquid–vapor interface (ψ) acting on the wetted surface projection (denoted by F_ψ in Fig. 4a).

As the aggregates coalesce in response to the applied capillary force, the liquid meniscus reconfigures itself to a lower energy state. At a constant matric potential, the change in energy state (energy release) by the liquid meniscus associated with an infinitesimal coalescence (dh) is given by (Ghezzehei and Or, 2000)

$$\mathrm{d}E_S|_\psi = \sigma_{LV}\frac{\partial \mathrm{SA}_{LV}}{\partial h}\,\mathrm{d}h \tag{7}$$

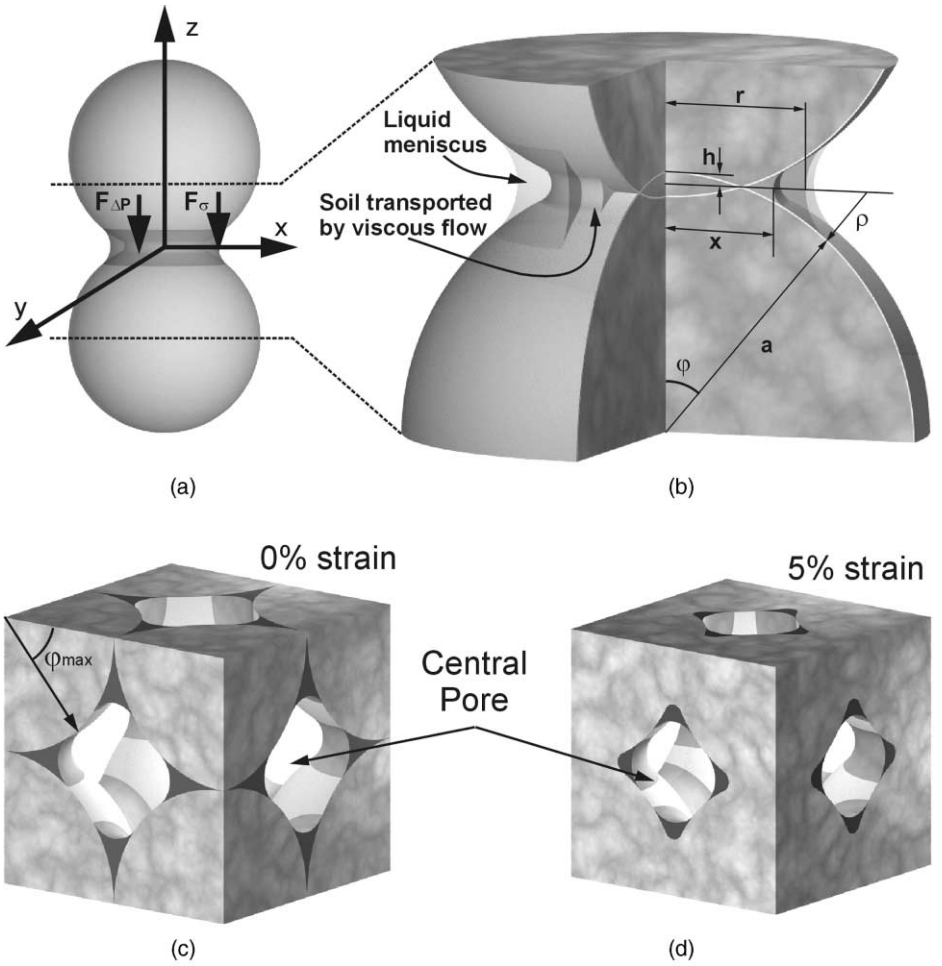

Fig. 4. The basic geometrical model for soil aggregate coalescence: (a) a pair of equal-sized aggregates in a 3D Cartesian coordinate system, and tensile forces acting along the contact area; (b) definition of basic geometric variables in a cross-section. Cubic packing (c) before and (d) after coalescence.

where $dE_S|_\psi$ defines the energy differential at constant ψ, SA_{LV} the surface area of the liquid–vapor interface. Ghezzehei and Or (2000) have derived an approximate expression for the rate of energy release:

$$F_{LV} \equiv \sigma_{LV} \frac{\partial SA_{LV}}{\partial h} = \left\{ A + B \ln\left(\psi \frac{a}{\sigma_{LV}}\right) + C\frac{h}{a} \right\} a\sigma_{LV} \quad (8)$$

The dimensionless fitting parameters for a pair of equal-sized spherical aggregates were found by regression analysis to be $A = 10.873$, $B = 0.3887$, $C = -4.891$ (with $r^2 = 0.991$). Then, the rate of energy release is given as

$$\frac{dE_S}{dt} \equiv \frac{dE_S}{dh}\frac{dh}{dt} = F_{LV}\frac{dh}{dt} \quad (9)$$

The process of coalescence by viscous flow of soil material at the inter-aggregate contact involves dissipation of energy. The rate of viscous energy dissipation (dE_V/dt) is given by (Ghezzehei and Or, 2000; Mackenzie and Shuttleworth, 1949)

$$\frac{dE_V}{dt} = 3\frac{\eta}{a^2}\left(\frac{dh}{dt}\right)^2 V \quad (10)$$

where $V = 4\pi a^3/3$ is the volume of the aggregate pair participating in the flow and η the viscosity of the soil as defined in (4).

From the assumption of incompressibility of the individual aggregates stated above, and basic principles of continuum mechanics, it is possible to formulate a relationship between the axial strain rate and shear rate (Mackenzie and Shuttleworth, 1949)

$$\dot{\gamma} = \frac{\sqrt{2}}{a}\frac{\mathrm{d}h}{\mathrm{d}t} \tag{11}$$

Substituting Eqs. (4) and (11) into Eq. (10) and integrating over the volume of a pair of aggregates leads to total energy dissipation equation due to flow

$$\frac{\mathrm{d}E_\mathrm{V}}{\mathrm{d}t} = 8\pi a\eta_\mathrm{p}\left(\frac{\mathrm{d}h}{\mathrm{d}t}\right)^2 + 4\sqrt{2}\pi a^2\tau_\mathrm{y}\frac{\mathrm{d}h}{\mathrm{d}t} \tag{12}$$

Eq. (12) represents the rate of energy dissipation from an aggregate pair as it coalesces (energy dissipates in the form of heat).

2.2.4. Constitutive relations for rate of aggregate deformation

When the only driving forces for coalescence are of capillary origin, energy dissipated due to viscous deformation of wet soil aggregates is provided by reconfiguration of the LV interface. Restated in terms of rate of energy change, the rate of energy gain by liquid reconfiguration ($\mathrm{d}E_\mathrm{S}$) is equal to the rate of energy dissipation by viscous deformation (flow) of aggregates ($\mathrm{d}E_\mathrm{V}$).

$$\frac{\mathrm{d}E_\mathrm{S}}{\mathrm{d}t} = -\frac{\mathrm{d}E_\mathrm{V}}{\mathrm{d}t} \tag{13}$$

Eq. (13) is the core of Frenkel's (1945) viscous sintering theory. For the aggregate rejoining problem we equate (9) and (12), and rearrange to obtain a general, first-order ordinary differential equation for rate of coalescence:

$$\frac{\mathrm{d}h}{\mathrm{d}t} = \frac{a}{2\eta_\mathrm{p}}\left(\frac{1}{4\pi a^2}F_\mathrm{LV} - \sqrt{2}\tau_\mathrm{y}\right) \tag{14}$$

where F_LV is as given by (8). The first term on the right-hand side of (14) states that the strain rate is proportional to capillary force (F_LV). The second term denotes the resistance of the soil to deformation (strength). Finally, (14) also shows an inverse relationship between the rate of coalescence ($\mathrm{d}h/\mathrm{d}t$) and the plastic viscosity (η_p).

The capillary force exerted upon the aggregate pair always pulls them towards the contact plane, leading to positive aggregate coalescence. Thus, (14) holds only when the right-hand side is positive, i.e.,

$$F_\mathrm{LV} \geq 4\sqrt{2}\pi a^2\tau_\mathrm{y} \tag{15}$$

The above mathematical condition defines the onset and termination of aggregate coalescence. For example, during drying of initially very wet (e.g., saturated) soil, aggregate deformation does not start until the capillary forces exceed the yield stress. Once this limit is exceeded (i.e., (15) is satisfied), deformation commences as defined by Eq. (14). The decrease in F_LV with strain (see (8) for details), and/or, increase in τ_y due to drying at a latter time, result in termination of aggregate coalescence.

A general solution to (14) is given by Ghezzehei and Or (2000)

$$\varepsilon(t) = \varepsilon_0\exp[F(t)] + \exp[F(t)]\int_{t_0}^{t}\exp[-F(t)]g(t)\,\mathrm{d}t \tag{16}$$

where

$$\varepsilon(t) = \frac{h(t)}{a}, \qquad f = \frac{\sigma_\mathrm{LV}C}{8\pi a}\frac{1}{\eta_\mathrm{p}},$$

$$g = \frac{1}{2\eta_\mathrm{p}}\left\{\frac{\sigma_\mathrm{LV}}{4\pi}\left[A + B\ln\left(\frac{a}{\sigma_\mathrm{LV}}\psi\right)\right] - \sqrt{2}\tau_\mathrm{y}\right\},$$

$$F(t) = \int_{t_0}^{t} f(t)\,\mathrm{d}t$$

and $\varepsilon_0 = h(0)/t$ is the initial strain level. Note two typographical errors in the original terms f and g presented in Eq. (8) of Ghezzehei and Or (2000).

Evaluation of (16) depends upon the particular forms of the equations used to describe soil rheological properties $\tau_\mathrm{y}(\psi)$, and $\eta_\mathrm{p}(\psi)$, as well as the $\psi(t)$ function. The rheological functions can be obtained from independent laboratory measurements, whereas the matric potential function depends on the wetting and drying processes to which the soil is subjected.

2.2.5. Illustrative examples

Detailed discussion on rheological characterization of wet soils is reported by Ghezzehei and Or (2001). In

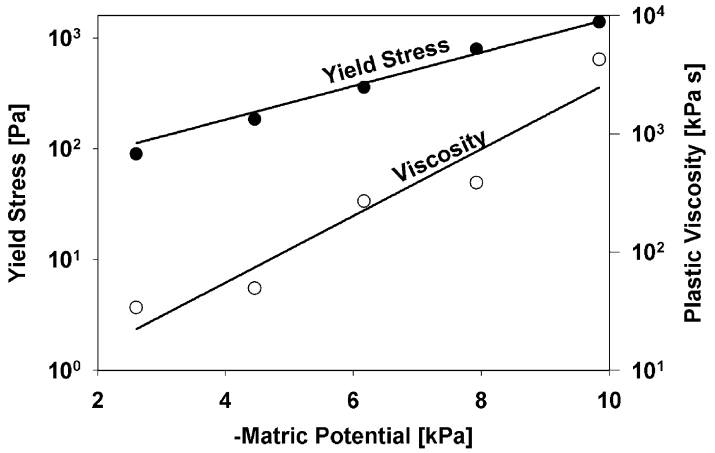

Fig. 5. The coefficient of viscosity and yield stress of Millville silt loam soil as function of matric potential. Solid lines are linearized best fits of Eqs. (17) and (18).

order for the rheological data obtained at discrete water contents (see Fig. 2) to be useful in evaluating (16), it was transformed into continuous functional form dependent on matric potential. The water contents were converted to matric potentials by using the soil bulk density and soil water characteristic of the Millville silt loam soil (Or, 1990). The resulting functional relationships between the Bingham model parameters and matric potential (Fig. 5) were fitted using two-parameter exponential equations

$$\eta_p = a_\eta \exp(b_\eta \psi) \tag{17}$$

$$\tau_y = a_\tau \exp(b_\tau \psi) \tag{18}$$

The fitting parameters of Eqs. (17) and (18) for Millville silt loam soil are $a_\eta = 5.6 \times 10^4$ Pa s, $b_\eta = 3 \times 10^{-4}$ Pa^{-1}, $a_\tau = 35$ Pa s and $b_\tau = 3 \times 10^{-4}$ Pa^{-1}, the r^2 values were 0.95 and 0.99, respectively.

Applications of the model developed in previous sections are illustrated for a basic element formed by cubic packing of equal-sized aggregates (Fig. 4c and d). The matric potential range that can support capillary liquid in the inter-aggregate pore space of the unit cell (Fig. 4c and d) is bound by lower and upper limits. The critical minimum potential corresponds to the LV interface with the radius of the liquid-neck (r) equal to that of the solid-neck (x). The maximum matric potential supporting capillary liquid is associated with largest liquid-neck radius (r) before the liquid–vapor interfaces of adjacent contacts touch each other. At matric potential values higher than the critical maximum, the central pore is completely filled with liquid, irrespective of the strain level (Mason and Morrow, 1990). The major and minor radii of curvature of the liquid–vapor interface at the upper and lower bounds of matric potential for a given strain state are shown in Table 1 (Ghezzehei and Or, 2000).

2.2.5.1. Aggregate coalescence for constant matric potential. The simplest situation for aggregate coalescence is where aggregates are subjected to constant matric potential. This situation can be developed under experimental conditions, where an infinitesimally thin soil sample (aggregate pack) is kept in equilibrium with a reservoir of water at a controlled energy level. Under these conditions, soil

Table 1
Radii of liquid–vapor interface defining minimum and maximum matric potential bounds for equal-sized spherical aggregates under cubic packing. The corresponding matric potential is calculated using (5)

ψ_{min}	ψ_{max}
$r_{min} = a\left(\frac{\sqrt{\varepsilon}}{a_p\sqrt{\varepsilon} - b_p}\right)^a$	$r_{max} = a\left(2 - \varepsilon - \frac{1-\varepsilon}{\cos(\varphi_{max})}\right)^b$
$\rho_{min} = \frac{a(2\varepsilon - \varepsilon^2) - r_{min}^2}{2(r_{min} - a)}$	$\rho_{max} = a(1-\varepsilon) - r_{max}$

[a] $a_p = 0.1080$, $b_p = 0.4939$ (fitting parameters with $r^2 = 0.999$).
[b] $\varphi_{max} = 45^\circ$, where φ is expansion angle of the liquid meniscus as defined in Fig. 4b (Gvirtzman and Roberts, 1991).

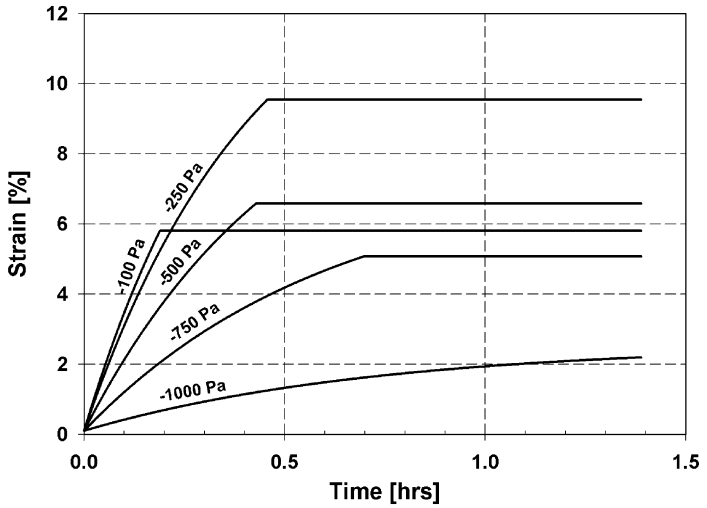

Fig. 6. Coalescence of soil aggregate pair 2 mm in diameter subjected to constant matric potential.

rheological properties remain constant, with the only variable element in the problem being the solid-neck configuration. In this scenario (16) is simplified to

$$\varepsilon(t) = \left(\varepsilon_0 + \frac{g}{f}\right)\exp(ft) - \frac{g}{f} \tag{19}$$

Sample calculations of aggregate coalescence under constant matric potential using rheological properties of Millville soil and 0% initial strain are depicted in Fig. 6 for different values of constant matric potential (expressed as matric suction). A decrease in matric potential (more negative values) is shown to decrease the slope of aggregate coalescence rates. This is explained by the increase in soil viscosity associated with dryer conditions. Under the wettest conditions (-100 and -250 Pa), cessation of aggregate coalescence is due to fill-up of the central pore by liquid (water). For the remaining dryer conditions (-500, -750 and -1000 Pa), coalescence terminates when the curvature of pendular LV interface overlaps the solid-neck.

2.2.5.2. Aggregate coalescence for a linear drying rate. Soil drying by internal drainage, evaporation and plant water uptake is another simple scenario we consider. The actual path of matric potential may be a complicated function of time, depending on environmental conditions, initial inter-aggregate strain and wetness status. In the wetness range where capillary driven aggregate coalescence is of importance (i.e., near saturation), wetting–drying processes can be described by simple cyclic functions. For this illustration, we consider subjecting initially saturated aggregates to low-amplitude cycles of linear drying for 30 min, i.e.,

$$\psi(t) = \vartheta t \tag{20}$$

where ϑ defines the rate of soil drying, followed by rapid (instantaneous) re-wetting, after which the aggregates are held at a constant head for 30 min as shown in Fig. 7a. The corresponding aggregate coalescence (strain) is depicted in Fig. 7b.

Aggregate coalescence during drying involves interplay between the increase in capillary forces (6) on one hand, and increase in viscosity (17) and yield stress (18) on the other hand. Aggregate coalescence begins only when the capillary forces exceed the yield stress of the soil aggregates, and continues at a rate inversely proportional to the viscosity, until it finally ceases when the yield stress once again overcomes the capillary forces.

2.3. Aggregate welding by steady external stress

2.3.1. Extension of capillary-induced coalescence model to welding by external stress

The mechanisms governing soil aggregate coalescence under internal capillary force and external

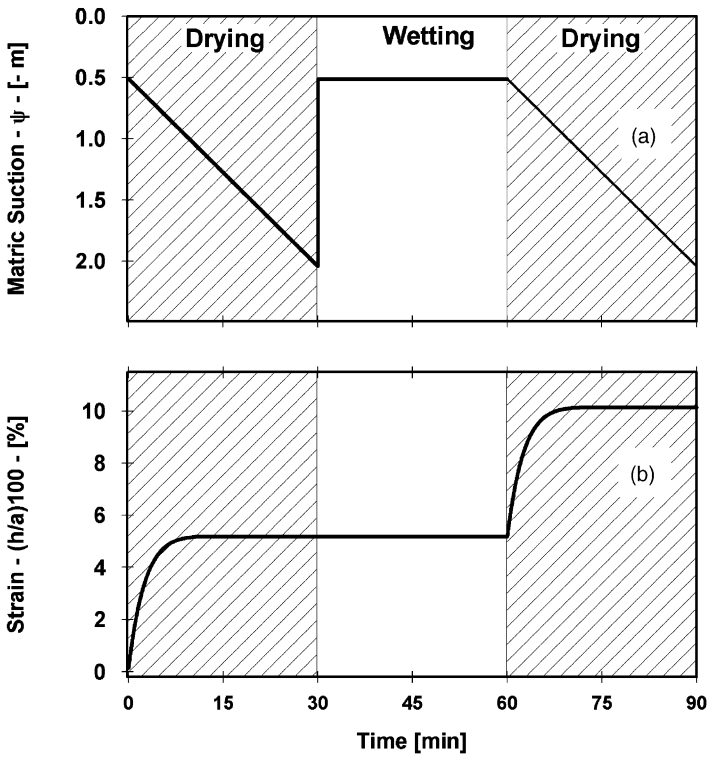

Fig. 7. (a) Matric suction during wetting and drying cycles which drives the aggregate coalescence process and (b) the resulting axial strain of a unit cell (0.1 mm aggregates) as function of time.

steady force are identical. The major difference between the two modes of force is that a steady capillary force acting upon an aggregate pair induces equal stresses at all contacts regardless of their spatial orientation, provided the aggregates have identical geometry and are at equal capillary pressure (Ghezzehei and Or, 2000). In contrast, an external steady force induces varying degrees of stress at different contacts depending on the orientation of the contacts with respect to the direction of the force.

Consider an aggregate pair (Fig. 4) subjected to a constant external force F, causing aggregate coalescence at their contacts, and outward flow of the material forming the contact region. Consequently, the centers of the aggregates move towards the contact by h, and the axial strain is given by $\varepsilon = h/a$. The radius (x) of the resulting circular contact area, at time t, can be approximated by

$$x^2 = a^2\lfloor 1 - (1-\varepsilon)^2 \rfloor \approx 2a^2\varepsilon \tag{21}$$

Then, the axial stress (σ) acting upon the contact area is

$$\sigma(t) = \frac{F}{2\pi a^2 \varepsilon(t)} \tag{22}$$

Because the stress changes at a relatively slow rate, compared to the strain rate, we assume the deformation obeys Bingham law (3)

$$\sigma(t) = \frac{F}{2\pi a^2 \varepsilon(t)} = \lambda_\mathrm{p}\frac{\mathrm{d}\varepsilon(t)}{\mathrm{d}t} + \sigma_\mathrm{y} \tag{23}$$

The coefficient of plastic viscosity in compression ($\lambda_\mathrm{p} = 2\eta_\mathrm{p}(1+\upsilon)$ (Vyalov, 1986)) and the yield stress in compression ($\sigma_\mathrm{y} = \tau_\mathrm{y}/2$) are determined from rheological measurements, where υ is Poisson's ratio. The analytical solution to (23), subject to the initial condition $\varepsilon(t=0) = \varepsilon_0$ (initial strain), is given by

$$\varepsilon(t) = \frac{1}{Q}\left\{1 + \mathrm{Product}\log\left[(Q\varepsilon_0 - 1)\exp(Q\varepsilon_0 - 1) \times \exp\left(-\frac{Q\sigma_\mathrm{y}t}{\lambda_\mathrm{p}}\right)\right]\right\} \tag{24}$$

where $Q = (2\pi a^2 \sigma_y / F)$. The function Product $\log(z) = \omega$ is the solution to the non-linear expression $z = \omega e^{\omega}$ (Abramowitz and Stegun, 1974). In the illustrative examples section, application of (24) along with viscoplastic rheological properties of soil will be presented.

2.3.2. Illustrative example

The weight of an overlying soil layer (overburden) is an example of steady external force that exists in all soils. In this example, we consider a pair of identical soil aggregates (radius = 1 mm), with a very small initial strain ($\varepsilon_0 = 0.001$). The line connecting the centers of the aggregates is parallel to the direction of the weight force ($F = 1.63 \times 10^{-4}$ N). The compressive stress (22) acting upon the contacts is shown in Fig. 8a. Ignoring all the interactions with neighboring aggregates, the strain induced by the stress is given by (24). In Fig. 8b, (24) is evaluated using viscoplastic properties of Millville silt loam soil (water content = 0.28 kg/kg, $\tau_y = 1225$ Pa, $\eta_p = 60$ kPa) and assuming $\upsilon = 0.5$.

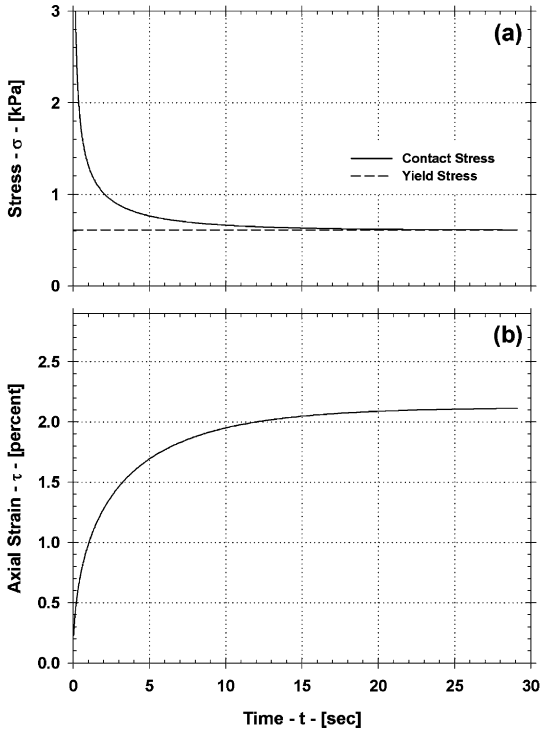

Fig. 8. Stress–strain relationships in aggregate pair model (Millville silt loam soil at 0.28 kg/kg water content) subjected to steady state stress: (a) applied contact stress and yield stress functions; (b) viscoplastic strain response as a function of real time.

The Bingham rheological model states that aggregate coalescence occurs only when the applied stress is greater than the yield stress ($\sigma_y = 612$ Pa). Initially, when the inter-aggregate contact area is nearly 0, the effective stress acting upon the contacts is very high (Fig. 8a), resulting in a rapid rate of aggregate coalescence (slope of Fig. 8b). As the contact area increases with time, the contact stress, hence the rate of aggregate coalescence, decreases. The coalescence ceases when the effective stress equals the yield stress. Further coalescence can be initiated only if the water content is increased (thereby decreasing the yield stress), or the applied load (force) is increased.

3. Soil structural dynamics under transient stresses

3.1. Transient stresses in agricultural soil

Unlike steady state stress, transient stresses (e.g., passage of farm implements) act upon soil for short durations. For example, rear wheels of a typical tractor operating at 5 m/h apply stress on the soil bed for less than 0.2 s (Harris, 1971). The amount of input energy that could dissipate by viscous flow of soil during such a short time of stress application is limited, thus part of the energy is stored in the form of elastic strain. The viscous component of the strain is permanent, while the elastic part is restored when the stress is removed (after the tractor passes). The partitioning of strain to recoverable and non-recoverable components during transient loading of loessal Luvisol by a tractor is illustrated in Fig. 9 (Horn and Baumgartl, 1999). The curves represent the location of a reference point, initially located at 100 mm below the ground surface. The overall strain path, including viscous and elastic deformations, is represented by the position of the observation point. The strain reaches maximum while the tractor weight is still acting. After the tractor has passed, however, strain that involved viscous flow is sustained permanently, while the remaining portion of strain that involved elastic energy storage is recovered. Note also that similar trends of deformation occur laterally at lower magnitudes.

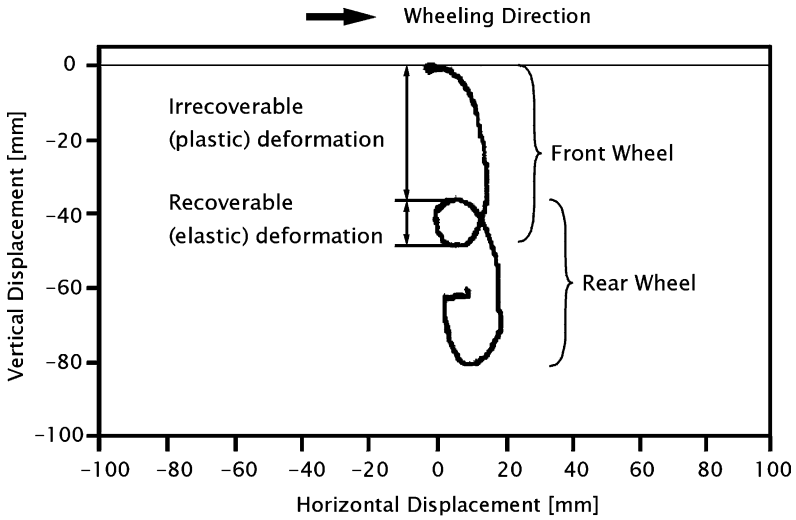

Fig. 9. The loci of observation points, initially 100 mm below the ground surface, during passage of the front and rear wheels of a tractor (Horn and Baumgartl, 1999).

3.2. Rheological properties of soil under transient stress

Rheological characterization of soil under transient stress mimics loading of soil under cyclic stresses. Using the measurement setup discussed above (Section 2.1.2), soil samples were subjected to sinusoidal shearing stress (τ) of angular velocity $\omega = 2\pi f$ (where f is frequency), and stress amplitude τ_0 (Fig. 10)

$$\tau = \tau_0 \sin(\omega t) \tag{25}$$

The instrument determines the resulting periodic shear strain and shear rate, which can be written in general form as

$$\gamma = \gamma_0 \sin(\omega t + \delta) \tag{26a}$$

$$\dot{\gamma} = \frac{\mathrm{d}\gamma}{\mathrm{d}t} = \gamma_0 \omega \cos(\omega t + \delta) \tag{26b}$$

where γ_0 is the strain amplitude. The phase shift angle, δ, sometimes called the "mechanical loss angle" (Dealy, 1982), describes the relative proportion of elastic and

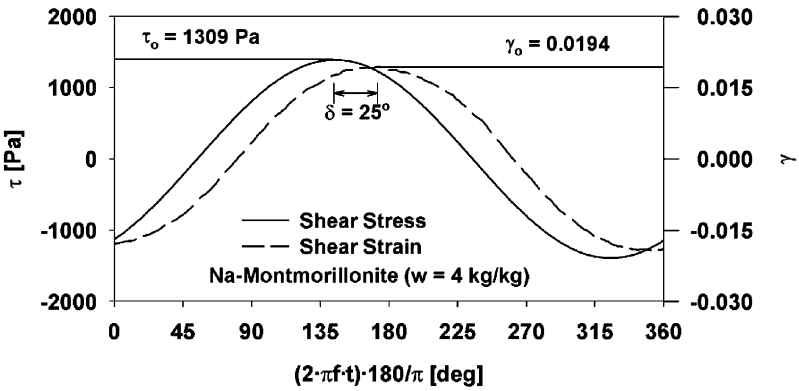

Fig. 10. Typical measurement results of oscillatory (transient) rheological measurement of Na-montmorillonite at frequency of 3.16 Hz, and water content of 4 kg/kg.

viscous deformations. A typical measurement output for Na-montmorillonite (water content = 4 kg/kg) at specified stress amplitude ($\tau_0 = 1390$ Pa) and loading frequency ($f = 3.16$ Hz) is shown in Fig. 10. The time axis is scaled by the frequency (angular velocity) of loading, and is expressed in units of radians

$$\varphi = \omega t \tag{27}$$

A phase shift angle of $\delta = 0$ indicates a perfectly elastic property, while $\delta = \pi/2$ indicates a perfectly viscous property. For most natural materials that exhibit intermediate behavior between ideal elastic solids and ideal viscous fluids, including soil, the phase shift angle is intermediate ($0° < \delta < 90°$). It is mathematically convenient and compact to represent the complementary viscous and elastic properties (viscoelastic) in a complex plane system as shown below.

The stress- and strain-amplitudes (τ_0 and γ_0 in (26a) and (26b), respectively) can be related by an equation of elasticity

$$G^* = \frac{\tau_0}{\gamma_0} \tag{28}$$

where $G^* = |G' + \mathrm{i}G''|$ is a complex shear modulus. The real component of the modulus $G' = G^* \cos(\delta)$, indicates ''storage'' (elastic) modulus which is related to the recoverable deformation. The imaginary component $G'' = G^* \sin(\delta)$, denotes the ''loss'' (viscous) modulus representing the irrecoverable deformation. The terms loss and storage refer to the fact that energy input for deformation dissipates if it is viscous and is stored if it is elastic, respectively.

Similarly, the stress- and strain-rate amplitudes (τ_0 and $\gamma_0\omega$ in (25) and (26b), respectively) can be related by an equation of viscosity similar to (1)

$$\eta^* = \frac{\tau_0}{\gamma_0 \omega} \tag{29}$$

where $\eta^* = |\eta' + \mathrm{i}\eta''|$ is complex viscosity. The imaginary component $\eta'' = \eta^* \sin(\delta)$, indicates the loss (dynamic) viscosity and the real component $\eta' = \eta^* \cos(\delta)$, denotes storage (elastic) viscosity.

Summarized viscoelastic properties (complex viscosity η^* and phase shift angle δ) for Millville silt loam soil are presented in Fig. 11.

Detailed discussions on the effects of stress magnitude, clay/soil type, water content, and loading frequency on the viscoelastic parameters are given by Ghezzehei and Or (2001).

3.3. Aggregate coalescence under transient stress

To enable the use of rheological properties presented above, it is necessary to represent the transient load of a tractor tire by an equation similar to (25). The pressure distribution under a moving tractor tire can be approximated by sinusoidal function as shown in Fig. 12 (e.g., see pressure distribution under smooth tire for soft soil in (VandenBerg and Gill, 1962)). When the force is observed from a fixed reference point, it is also sinusoidal with respect to time

$$F = F_0 \sin(\omega t) \tag{30}$$

where F_0 is the maximum (amplitude) force induced when the tractor is overhead. The angular velocity ω is related to the dynamic contact length (L) and tractor speed (V_T) by

$$\omega = 2\pi \left(\frac{V_\mathrm{T}}{2L} \right) \tag{31}$$

The division by two inside the parentheses in (31) is because the force function makes only a half sine-cycle.

3.3.1. Geometrical model: modification to Hertzian strain

Most geophysical models of deformation of particulate media (e.g., sandstone grains) consider the contact area of two spherical bodies (Fig. 13) resulting from an entirely elastic deformation as modeled by Hertz theory (e.g., Mavko et al., 1998). According to the Hertzian model, the strain flattens the contact areas without affecting other portions of the spheres (Fig. 13b). Considering that flow of soil material at aggregate contacts involves viscous flow and irreversible energy dissipation (as discussed above) (Ghezzehei and Or, 2001) require a different conceptual picture for the deformation process. We thus propose that elastic deformation of a soil aggregate pair results in bulging of the aggregates without permanent flow (rearrangement) of soil material around the contact (Fig. 13c) with the magnitude of the axial strain being equal to the Hertzian strain. Consequently, when an aggregate pair is subjected to oscillatory stress, the

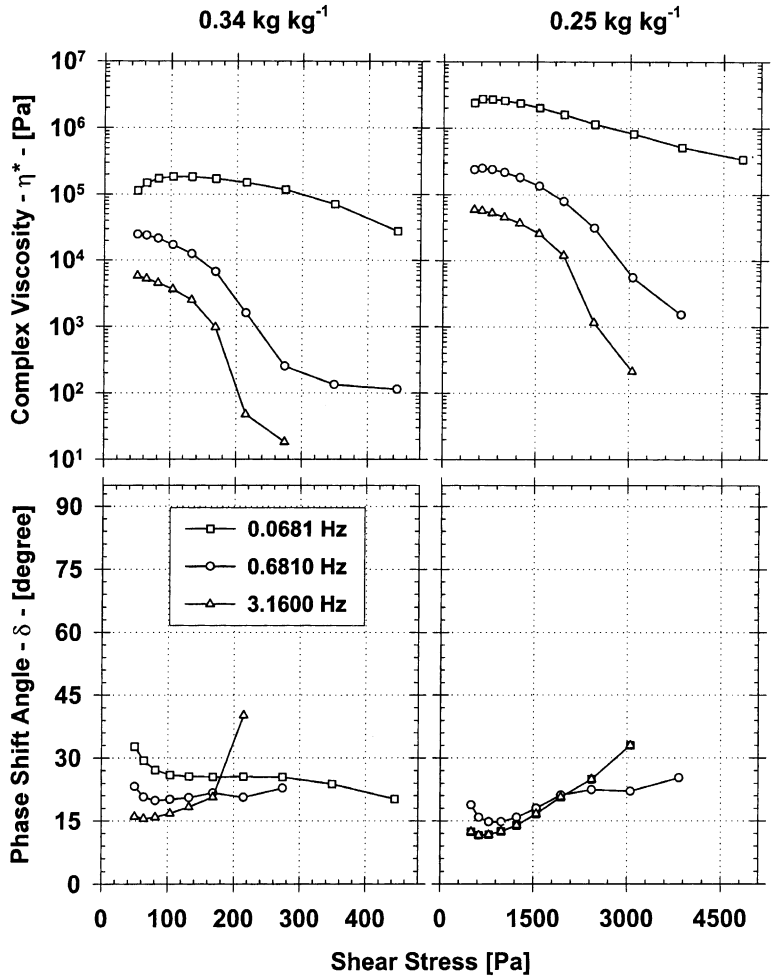

Fig. 11. Summary of viscoelastic properties of Millville silt loam soil. Each point in the plots denotes the mean of three independent replicates.

aggregates undergo elastic bulging while soil material at the contacts flows viscously. The elastic deformation is instantaneous while the viscous flow takes place at a rate dictated by wet soil viscosity.

When the applied axial force (30) presses the two aggregates together (Fig. 13), the resulting elastic strain (ε_e) at any time (t) is given by (Ghezzehei and Or, 2001)

$$\varepsilon_e(t) = \sqrt[3]{\frac{9}{512}\left(\frac{1-\upsilon}{a^2 G'}\right)^2 [F_0 \sin(\omega t)]^{2/3}} \tag{32}$$

The deformation (flow) at the inter-aggregate contact is considered entirely viscous as stated by (23) without yield stress (i.e., $\sigma_y = 0$). The solution to (23), with time-dependent input force (30), is given by

$$\varepsilon_v(t)^2 = \frac{F_0}{2\pi^2 a^2 f \lambda'}(1 - \cos[\omega t]) + \varepsilon_0^2 \tag{33}$$

where $\lambda' = 2\eta'(1+\upsilon)$ (Vyalov, 1986) is the "loss" component of the complex viscosity (29). The overall axial strain is given by the sum of the elastic (32) and viscous (33) components:

$$\varepsilon(t) = \varepsilon_e(t) + \varepsilon_v(t) \tag{34}$$

The applications of soil viscoelastic rheological properties and the above models (34) is demonstrated in the

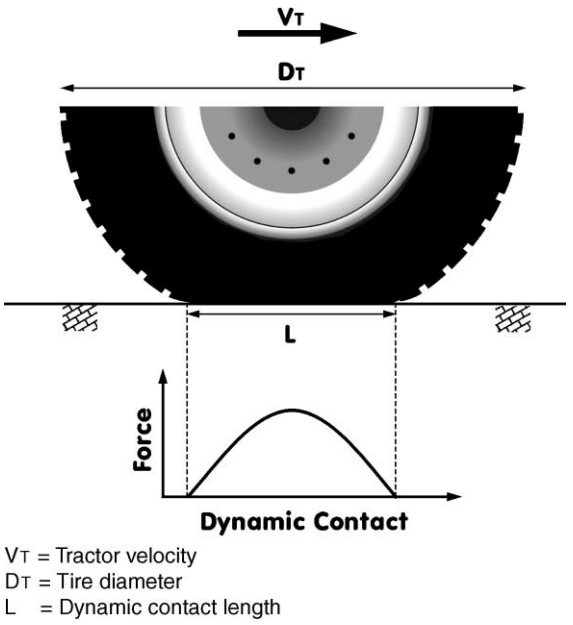

Fig. 12. Longitudinal stress distribution under a moving tractor tire. V_T and D_T stand for velocity and diameter of the tire. L is the contact length in the direction of the tire motion.

subsequent section using an example that mimics the effects of fast- and slow-passage of a tractor.

3.3.2. Illustrative example: soil aggregate coalescence under transient load

The most common oscillatory stresses that occur in natural agricultural soils result from passage of farm implements. The force delivered by a tractor can be denoted by a half-cycle sine function, (30). Qualitatively, the frequency (f) of the sine function is proportional to tractor speed, and the force amplitude (F_0) is proportional to the axle-load.

In the following example, we consider a vertically upright aggregate pair (radius, 1 mm) subjected to cyclic force ($F_0 = 1.63 \times 10^{-4}$ N) at two different tractor speeds (0.32 and 3.2 km/h). For simplicity, we also consider that the front and rear wheels are identical in size and axle-load. For this illustration, we consider a standard 11–38 tractor tire (diameter, 1.47 m and deflection, 0.038 m) with a dynamic contact line $L = 0.468$ m (VandenBerg and Gill, 1962). The tractor speed (V_T) is translated to angular velocity (ω) of the force function (30) as shown in (31).

Ignoring all interactions with neighboring aggregates and effect of depth (downward stress propagation), the strain induced by the passing tractor as a function of time is given by (34). For the purpose of comparing different tractor speeds that induce stresses of different periods, the time (t) is scaled by the frequency as in (27) and is expressed in units of degrees. The applied oscillatory force (30) is symmetric about F_0 as shown in Fig. 14a. The resulting oscillatory stress, however, is asymmetric (skewed to the right) because it also depends on the increasing strain magnitude. The total strains in a soil aggregate pair (Millville silt loam soil, water content = 0.28 kg/kg) subjected to front- and rear-tractor wheel impact are depicted in Fig. 14b.

The viscous strain amplitude occurring at the inter-aggregate contacts lags behind the stress amplitude by $\pi/2$ radians, and the elastic bulging of the aggregates is in phase with the stress curve as shown in Fig. 14b. The magnitude of the strain components are determined by compound effects of the complex viscosity (η^*) and phase shift angle (δ). In Fig. 14b and c, it is indicated that strains at 3.2 km/h are slightly lower than at 0.32 km/h. Physically, this implies that longer loading time, during slow passage of a tractor, provides enough opportunity for more viscous straining to occur. The higher phase shift angle (δ) at lower frequency shown in Fig. 11 also suggests a more viscous strain (less elastic) component. In general, the increase in contact area with each additional loading cycle decreases the effective stress. Consequently, the degree of viscous strain also decreases

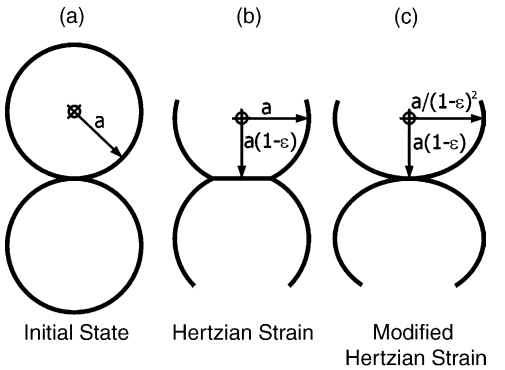

Fig. 13. Elastic strain in aggregate pair model: (a) aggregate pair model before strain; (b) aggregate pair model under Hertzian strain; (c) aggregate pair model under modified Hertzian strain.

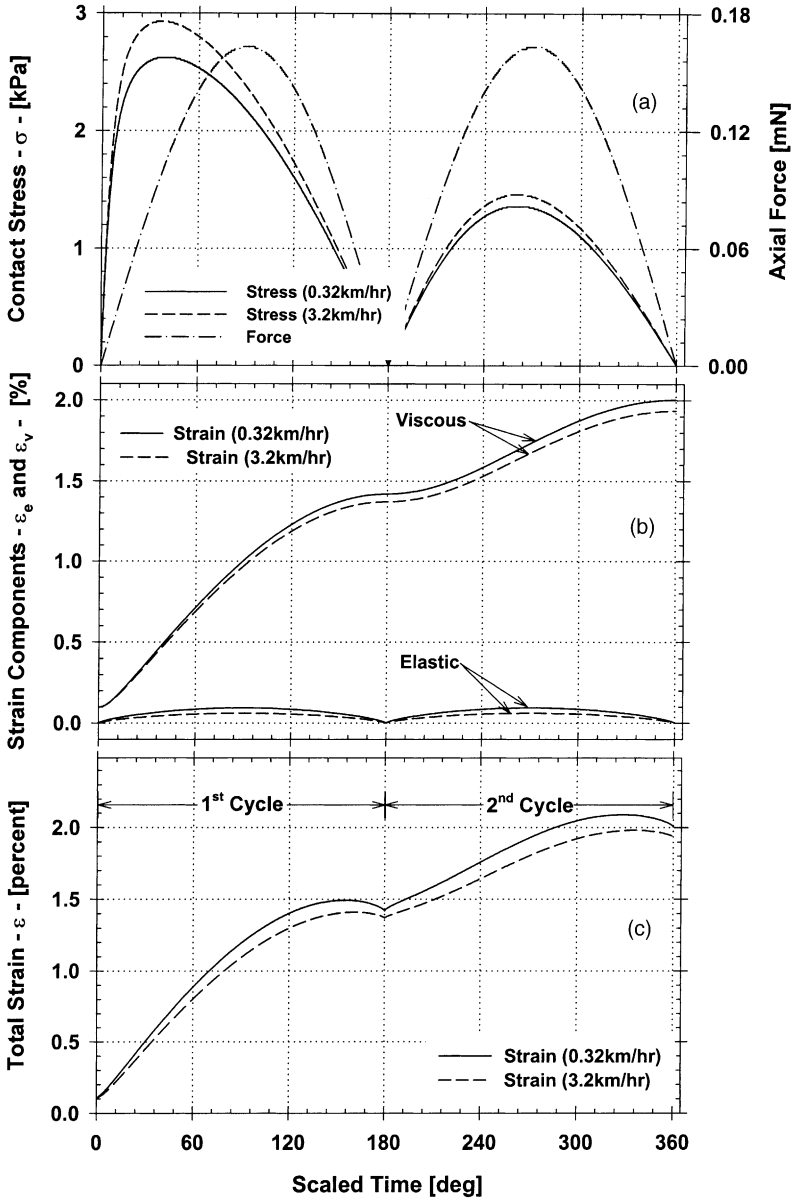

Fig. 14. Stress–strain relationships in aggregate pair model (Millville silt loam soil at 0.28 kg/kg water content) subjected to front- and rear-wheel passes by a tractor (tire diameter, $D = 1.47$ m) at velocities of 0.32 and 3.2 km/h. (a) Applied cyclic force and contact stress, (b) elastic and viscous strain components and (c) total strain as functions of scaled time (in radians).

with the number of cycles. Practically, this implies that the incremental damage incurred by a tractor passing over aggregated soil decreases with the number of passes. Thus, the particular aggregate geometry and soil rheology define the maximum strain level that can be caused by a given stress condition.

4. Upscaling to soil aggregate bed: future outlook

The models presented in this review deal with discrete representation of the soil aggregates that applies only to the initial loose state of soil aggregate bed, in which adjacent inter-aggregate contacts are not

overlapping and flow at the contacts is radially symmetrical. After a certain cut-off strain value $\varepsilon_c = 0.12$ (Ghezzehei and Or, 2000) has been reached, adjacent contact regions begin to interfere each other, and deformation beyond such point occurs by flow of soil through more restricted paths. Deformation in a unit cell with overlapping contacts involves asymmetric complex flow path. Flow continues in such restricted flow paths until eventually the differential flow results in closed and spherical pores. Recently, we proposed to use an adaptation of a model developed by Mackenzie and Shuttleworth (1949) for the later stages of deformation involving shrinkage of spherical pores (Ghezzehei and Or, Stress-induced shrinkage of isolated soil pores, 2001, submitted for publication). The model considers shrinkage of spherical pores embedded in a uniform Newtonian-viscous or Bingham-viscoplastic soil matrix.

Derivations presented in the preceding sections focused on the dynamics of a single unit cell. Proper quantification of structural dynamics in a profile of soil aggregate bed requires upscaling of these unit cell models to multiple cells and contacts. For aggregate coalescence due to internal capillary forces, the stresses are generated locally at inter-aggregate contacts and are omnidirectional. Therefore, upscaling of unit cell calculations to aggregate bed requires only the knowledge of matric potential profile, and consideration of the aggregate size distribution. In contrast, external forces originate at specific position on the profile (usually at the top) and they have specific direction. Therefore, upscaling of unit cell calculations under external stresses require further description of spatial arrangement of unit cells and stress transmission between adjacent unit cells. In order to perform the upscaling in a mathematically tractable way, without resorting to homogenization and continuum approaches, we propose to use simplified spatial structure of unit cells and employ a sufficiently simple description of force and stress transmission between adjacent unit cells (Ghezzehei and Or, Dynamics of pore space in soil aggregate bed under static and dynamic external loads, 2001, submitted for publication). We represent a bed of soil aggregates by a vertical one-dimensional stack of rhombohedral unit cells. Each unit cell represents a monolayer of aggregates as shown in Fig. 15a and b.

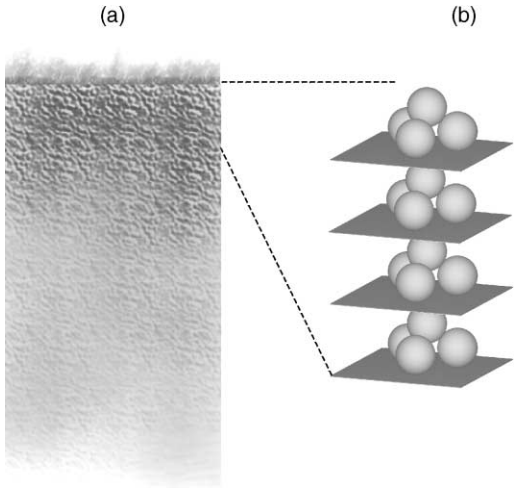

Fig. 15. Conceptual scheme for upscaling unit cell models to soil profile: (a) proposed spatial arrangement of soil aggregates; (b) force components for a randomly oriented unit cell.

The deformations in the rhombohedral unit cells in the different layers are described by the models presented in this review. Actual accounting for transmission of stresses from a layer of aggregates to the one underneath it requires consideration of all the geometric details. Such approach, if implemented could be useful to predict localization of stresses and strains in the aggregate bed (e.g., Blair et al., 2001; Calvetti and Emeriault, 1999; Huntley, 1998; Oron and Herrmann, 1999; Radjai et al., 1998). On the other hand, such an approach involves intensive numerical simulation. To retain the analytical capability of the present model, we employ a simple area-averaging approach for stress transmission. We introduce a conceptual rigid plane that carries the external load and uniformly distributes the stress to the unit cell underneath it. Similar conceptual rigid planes separate each layer. This amounts to summing up the weight carried by a layer and transmitting it uniformly to the layer below. The transmission of stresses is a time-dependent process, as determined by the soil rheology. Based on the rheological properties of soil discussed earlier, we recognize different forms of stress transmissions under steady and transient stresses.

Under steady state external stress, a soil aggregate bed exhibits a Bingham viscoplastic behavior. The soil material at every inter-aggregate contact flows radially outward, whenever the applied stress exceeds

the yield stress of the soil. Because the soil is considered to be under viscous condition, during such deformation, it accommodates the entire stress. The rate of deformation decreases with time as the inter-aggregate contact area increases, until it finally ceases when the contact stress σ equals the yield stress of the soil σ_y. At that instance, the entire magnitude of the stress is transmitted to the subsequent layer. Under transient loads, soil flow processes involve both elastic and viscous components. As described above, viscous flow accommodates the stresses during deformation, whereas the elastic deformation occurs instantaneously. As a result, the elastic stress component is transmitted to the subsequent layer immediately. If the stresses (δ or τ) are less than their corresponding yield values (δ_y or τ_y) or the layer reaches its ultimate density, then the viscous flow also ceases in which case the total stress would be transmitted to the subsequent layer.

5. Summary and conclusions

This work reviews recent developments in modeling post-tillage structural dynamics of aggregated soils. The basic premise behind these models is that subsequent to soil fragmentation by tillage, external and internal forces act to rejoin the aggregates, resulting in a more dense (pre-tillage) soil structure. We tacitly assume that most of the changes occur within the inter-aggregate pore space, whereas, at the time-scales considered, soil textural pore space remains unchanged.

The models combine basic physical principles for tractable soil geometries with measurable soil rheological properties, to predict rate of strain for different types of forces. Following tillage, the primary force in most agricultural soils is due to capillarity and it results from wetting and drying cycles (irrigation or rainfall). Additionally, passage of farm implements induce a very different stress regime that often operates for only a fraction of a second. Consequently, soil deformation and compaction is a strong function of the duration of the load and soil wetness, which largely determines the soil rheological properties. The applicability of the models to a real soil was illustrated for Millville silt loam. The review provides a brief description of proposed approaches for upscaling the unit cell to modeling the behavior of an aggregate bed.

Acknowledgements

The partial funding by USDA/NRI through contract No. 9700814, the US–Israel Binational Agricultural and Research Fund (BARD) through contract No. 2794-96 and the Utah Agricultural Experimental Station (UAES), Utah State University, Logan, UT, are gratefully acknowledged. Approved as UAES journal paper No. 8081.

References

Abramowitz, M., Stegun, I.A., 1974. Handbook of Mathematical Functions, with Formulas, Graphs and Mathematical Tables. Dover Publishers, New York.

Blair, D.L., Mueggenburg, N.W., Marshall, A.H., Jaeger, H.M., Nagel, S.R., 2001. Force distributions in three-dimensional granular assemblies: effects of packing order and interparticle friction (Art. No. 041304). Phys. Rev. E 6304 (4), 1304.

Calvetti, F., Emeriault, F., 1999. Interparticle forces distribution in granular materials: link with the macroscopic behaviour. Mech. Cohes.-Frict. Mater. 4 (3), 247–279.

Collis-George, N., Greene, R.S.B., 1979. The effect of aggregate size on the infiltration behavior of slaking soil and its relevance to ponded irrigation. Aust. J. Soil Res. 17, 65–73.

Day, P.R., Holmgren, G.G., 1952. Microscopic changes in soil structure during compression. Soil Sci. Soc. Am. Proc. 16, 73–77.

Dealy, J.M., 1982. Rheometers for Molten Plastics: A Practical Guide to Testing and Property Measurement. Van Nostrand Reinhold, New York, 302 pp.

Frenkel, J., 1945. Viscous flow of crystalline bodies under the action of surface tension. J. Phys. (Moscow) 9 (5), 385–391.

Gessinger, G.H., Fischmeister, H.F., 1972. A modified model for the sintering of tungsten with nickel additions. J. Less-common Met. 27, 129–141.

Ghavami, M., Keller, J., Dunn, I.S., 1974. Predicting soil density following irrigation. Trans. ASAE 17, 166–171.

Ghezzehei, T.A., Or, D., 2000. Dynamics of soil aggregate coalescence governed by capillary and rheological processes. Water Resour. Res. 36 (2), 367–379.

Ghezzehei, T.A., Or, D., 2001. Rheological properties of wet soils and clays under steady and oscillatory stresses. Soil Sci. Soc. Am. J. 65, 624–637.

Gvirtzman, H., Roberts, P.V., 1991. Pore scale spatial analysis of two immiscible fluids in porous media. Water Resour. Res. 27 (6), 1165–1176.

Harris, W.L., 1971. The soil compaction process. In: Barnes, K.K. (Ed.), Compaction of Agricultural Soils. American Society of Agricultural Engineering, St. Joseph, MI, pp. 9–44.

Heady, R.B., Cahn, J.W., 1970. An analysis of the capillary forces in liquid-phase sintering of spherical particles. Metall. Trans. 1, 185–189.

Hillel, D., 1998. Environmental Soil Physics. Academic Press, New York, 771 pp.

Horn, R., Baumgartl, T., 1999. Dynamic properties of soils. In: Sumner, M.E. (Ed.), Handbook of Soil Science. CRC Press, Boca Raton, pp. A19–A51.

Huntley, J.M., 1998. Fluidization, segregation and stress propagation in granular materials. Phil. Trans. R. Soc. London Ser. A 356, 2569–2590.

Keller, J., 1970. Sprinkler intensity and soil tilth. Trans. ASAE 13 (6), 118–125.

Kemper, W.D., Rosenau, R.C., 1984. Soil cohesion as affected by time and water content. Soil Sci. Soc. Am. J. 48, 1001–1006.

Koolen, A.J., 1983. Agricultural Soil Mechanics. Advanced Series in Agricultural Sciences. Springer, Berlin, 235 pp.

Kwaad, F.J.P., Mücher, H.J., 1994. Degradation of soil structure by welding—a micromorphological study. Catena 23, 253–268.

Mackenzie, J.K., Shuttleworth, R., 1949. A phenomenological theory of sintering. Proc. Phys. Soc. 62 (12B), 833–852.

Mason, G., Morrow, N.R., 1990. Capillary behavior of a perfectly wetting liquid in irregular triangular tubes. J. Colloid Interf. Sci. 141 (1), 262–274.

Mavko, G., Mukerji, T., Dvorkin, J., 1998. The Rock Physics Handbook. Cambridge University Press, Cambridge.

McMurdie, J.L., Day, P.R., 1958. Compression of soil by isotropic stress. Soil Sci. Soc. Am. Proc. 22, 18–22.

Mullins, C.E., MacLeod, D.A., Northcote, K.H., Tisdall, J.M., Young, I.M., 1990. In: Lal, R., Stewart, B.A. (Eds.), Hard-setting Soils: Behavior, Occurence, and Management. Soil Degradation. Springer, New York, pp. 37–108.

Or, D., 1990. Irrigation measurement considering soil variability and climatic uncertainty. Ph.D. Thesis. Utah State University, Logan, UT.

Or, D., 1996. Wetting induced soil structural changes: the theory of liquid phase sintering. Water Resour. Res. 32, 3041–3049.

Or, D., Wraith, J.M., 1999. Temperature effects on soil bulk dielectric permittivity measured by time domain reflectometry: a physical model. Water Resour. Res. 35 (2), 371–384.

Or, D., Leij, F.J., Snyder, V., Ghezzehei, T.A., 2000. Stochastic model for post-tillage soil pore space evolution. Water Resour. Res. 36 (7), 1641–1652.

Oron, G., Herrmann, H.J., 1999. Contact forces in regular 3D granular pile. Physica A 265 (3–4), 455–462.

Radjai, F., Wolf, D.E., Jean, M., Moreau, J.J., 1998. Bimodal character of stress transmission in granular packings. Phys. Rev. Lett. 80 (1), 61–64.

Silva, H.R., 1995. Wetting induced changes in near-surface soil physical properties affecting surface irrigation. Ph.D. Thesis. Utah State University, Logan, UT.

Sumner, M.E., Stewart, B.A., 1992. Soil Crusting: Chemical and Physical Processes. Advanced Soil Science Lewis, Boca Raton, FL, 372 pp.

VandenBerg, G.E., Gill, W.R., 1962. Pressure distribution between a smooth tire and the soil. Trans. ASAE 5, 105–107.

Vomocil, J.A., Folker, W.J., 1961. Effect of soil compaction on storage and movement of soil air and water. Trans. ASAE 4, 242–246.

Vyalov, S.S., 1986. Rheological Fundamentals of Soil Mechanics. Elsevier, Amsterdam, 565 pp.

Wiermann, C., Werner, D., Horn, R., Rostek, J., Werner, B., 2000. Stress/strain processes in a structured unsaturated silty loam Luvisol under different tillage treatments in Germany. Soil Till. Res. 53 (2), 117–128.